

Inverse four-wave-mixing and self-parametric amplification effect in optical fibre

Sergei K. Turitsyn^{1,2*}, Anastasia E. Bednyakova^{2,3}, Mikhail P. Fedoruk^{2,3},

Serguei B. Papernyi⁴ & Wallace R.L. Clements⁴

¹*Aston Institute of Photonic Technologies, Aston University, Birmingham, B4 7ET, UK*

²*Novosibirsk State University, Novosibirsk 630090, Russia*

³*Institute of Computational Technologies, SB RAS, Novosibirsk 630090, Russia*

⁴*MPB Communications Inc., Montreal, QC, H9R 1E9 Canada*

**Corresponding author: s.k.turitsyn@aston.ac.uk*

An important group of nonlinear processes in optical fibre involves the mixing of four waves due to the intensity dependence of the refractive index. It is customary to distinguish between nonlinear effects that require external/pumping waves (cross-phase modulation and parametric processes such as four-wave mixing) and self-action of the propagating optical field (self-phase modulation and modulation instability). Here, we present a new nonlinear self-action effect, self-parametric amplification (SPA), which manifests itself as optical spectrum narrowing in normal dispersion fibre, leading to very stable propagation with a distinctive spectral distribution. The narrowing results from an inverse four-wave mixing, resembling an effective parametric amplification of the central part of the spectrum by energy transfer from the spectral tails. SPA and the observed stable nonlinear spectral propagation with random temporal waveform can find applications in optical communications and high power fibre lasers with nonlinear intra-cavity dynamics.

Introduction

Nonlinear fibre optics is a research field at the two-way interface of fundamental nonlinear physics and fibre-optic engineering that encompasses diverse areas of science and technology. Nonlinear effects in optical fibre are critically important for various practical applications ranging from telecommunications to medical fibre lasers (see e.g. [1-6] and references therein). However, nonlinear fibre optics is also a remarkable and versatile test-bed for experimental probing of ideas and concepts of fundamental nonlinear science [5, 7-13]. This, in turn, means that fibre optics is an ideal platform for the invention and development of novel devices based on nonlinear design concepts with functionality not available in linear science engineering. Due to the relatively low threshold for the occurrence of nonlinear effects in fibre, they may adversely impact signal propagation in optical communications, or be positively exploited for the development of all-optical devices for optical networks, fibre lasers, signal processing components and in many other applications.

Typically, fibre nonlinear effects are subdivided into two main categories: phenomena induced by the nonlinearities that arise from scattering (stimulated Brillouin scattering (SBS) and stimulated Raman scattering (SRS)) and the nonlinear effects due to the Kerr effect, the intensity dependence of the refractive index (self-phase modulation (SPM), cross-phase modulation (XPM), four-wave mixing (FWM), modulation instability (MI) and parametric processes based on FWM [2, 4]). The interaction of two or more waves with different frequencies may lead to power transfer between them, according to the corresponding stimulated scattering or parametric processes. A subclass of such phenomena occurs in the degenerate case, when a single wave affects itself through the nonlinear response of the medium. This is called a self-action effect. Although the differentiation between various manifestations of the Kerr nonlinearity is somewhat artificial (as all elementary nonlinear processes resulting from the cubic nonlinearity formally can be treated as a mixing of four waves), from the practical view point, it is convenient to distinguish between nonlinear interactions of the optical field under consideration with

external fields (e.g. pumping waves) co-existing from the very outset (for instance, cross-phase modulation and parametric processes) and self-action of the propagating light wave (e.g. self-phase modulation and modulation instability).

In general, optical nonlinear self-action effects may be both spatial (self-focusing, self-phase modulation, spatial modulation instability) and temporal (self-phase modulation, temporal modulation instability). Self-action occurs when a propagating electromagnetic wave induces a refractive index change in the medium. The modified index of refraction in a fibre in turn affects the overall propagating field, producing effective self-action of the wave.

Optical parametric amplification (OPA) in fibres, pioneered by R. Stolen [14], is traditionally considered as a process of energy transfer from pumping wave(s) to a signal wave. Recently, fibre OPA has become a booming area of research with impressive demonstrations of the feasibility of low-noise parametric amplification in high-capacity optical communications [15-22]. These breakthroughs are greatly supported by recent progress in the development of efficient highly-nonlinear fibres with a large ratio of the nonlinear coefficient to the attenuation parameter.

In this work, we introduce a new nonlinear self-action effect in optical fibre, inverse FWM or self-parametric amplification (SPA), which occurs in normal dispersion optical fibres under certain conditions described below. Note that the term "parametric amplification" is employed here in a context different from the standard usage. Traditional parametric amplification is typically defined for monochromatic waves, while here we use this term for the relatively broad spectrum of a multi-longitudinal-mode Raman fibre laser. Moreover, here the term "amplification" means only a re-distribution of the energy due to inverse FWM and is applied only to the central part of the spectrum that is "gaining" power at the expense of the energy decrease in the spectral tails of the field. However, we believe that this terminology helps to explain the underlying elementary processes and physics of the unusual nonlinear process demonstrated. We observed experimentally and confirm through comprehensive numerical

modelling that the spectral width of a signal produced by a Raman fibre laser becomes narrower after propagation in a sufficient length of normal dispersion fibre. The resulting state, featuring a narrow spectrum and random temporal field distribution, propagates with remarkable stability, showing potential for applications in fibre lasers and optical communications. We present a basic theory of self-parametric amplification that is confirmed by extensive numerical modelling and experimental observations.

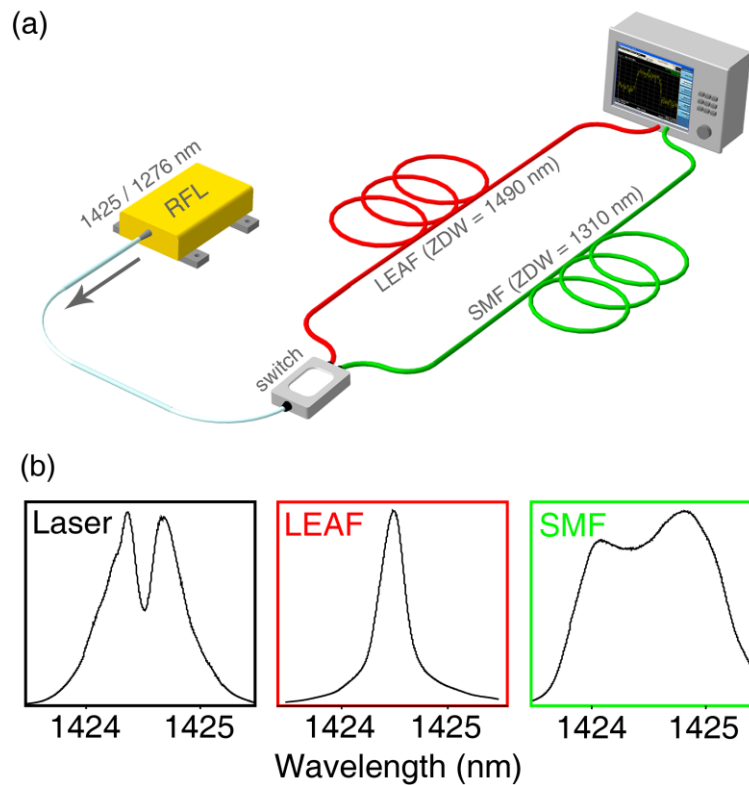


Figure 1. Experimental observation of spectrum evolution in normal and anomalous dispersion fibres. (a) Experimental setup. **(b)** Initial spectrum and spectrum after propagation in 100 km of LEAF and SMF-28 fibres. The power launched into each fibre was 1.5 W.

Results

Experimental setup. We start from the description of the experiment that initiated this study. The experimental setup is shown in Fig. 1(a). In the first set of experiments, the Raman fibre laser (RFL) [23] operated at ~ 1425 nm while, in the set of cross-check experiments presented at the end of the paper, an RFL operating at 1276 nm was used. Both Raman lasers operated in the continuous wave (CW) regime with a maximum output power up to 2W. The

outputs were randomly polarized with a degree of polarization $< 5\%$. It is widely known in fibre-optics that nonlinear effects such as four-wave mixing and self-phase modulation typically manifest themselves as a spectrum broadening when relatively high-power CW fields propagate in optical fibres [23-29]. A characteristic feature of the Raman fibre laser, related to high in-resonator power and the resulting in-cavity spectral broadening, is that its output spectrum has two peaks with a separation of 0.2 – 1 nm (Fig. 1b). The double-peaked structure of the output spectrum is the result of the FWM-induced spectral broadening inside the Raman converter cavity which leads to a spectral breadth which exceeds the reflection bandwidth of the fibre Bragg grating (FBG) output coupler and therefore to radiation “overflowing” the FBG reflector [23-29, 33].

The laser radiation generated at 1424.5 nm was launched into the 100-km long LEAF (Large Effective Area Fibre) or SMF-28 (Single Mode Fibre) fibres, with a zero-dispersion wavelength around 1490 nm for LEAF and 1310 nm for SMF-28. Thus, light propagates in the region of normal dispersion for the first and anomalous dispersion for the latter. The spectra at the input and output of the 100-km lengths of fibre were measured with an Optical Spectrum Analyzer (OSA) with a resolution of 0.01 nm.

Narrowing of the optical spectra. The measured optical spectrum at the end of LEAF fibre shows significant narrowing (see Fig. 1(b) - LEAF), in sharp contrast to the typical nonlinear spectral broadening in SMF-28 (see Fig. 1(b) - SMF) caused by four-wave mixing which has been observed and studied in a number of experimental and theoretical publications [23, 24, 27–31]. The explanation of this atypical narrowing effect is the aim of our work.

Extensive numerical modelling of light generation in the Raman fibre laser and its further propagation in the LEAF fibre fully confirms the observed unusual spectral behavior of a nonlinear wave in a long fibre with normal dispersion. Signal evolution inside the laser cavity was modelled by the set of coupled modified nonlinear Schrödinger equations taking into

account dispersion, Kerr nonlinearity, Raman gain, depletion of the Raman pump wave and fibre losses with all details of modelling presented, e.g. in [2, 32] (see also Methods section below). Signal evolution in the LEAF fibre was computed using the standard nonlinear Schrödinger equation [2].

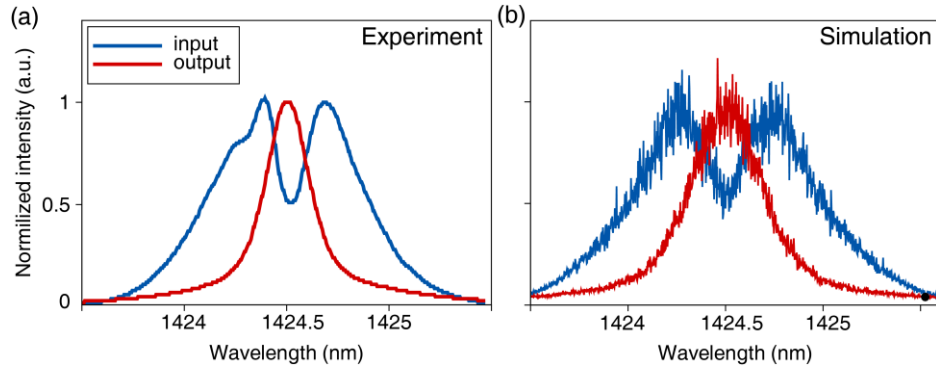


Figure 2. Spectrum shape after signal propagation in LEAF fibre. (a) experiment and (b) simulation. $P_0(0) = 1.5$ W, $L = 100$ km.

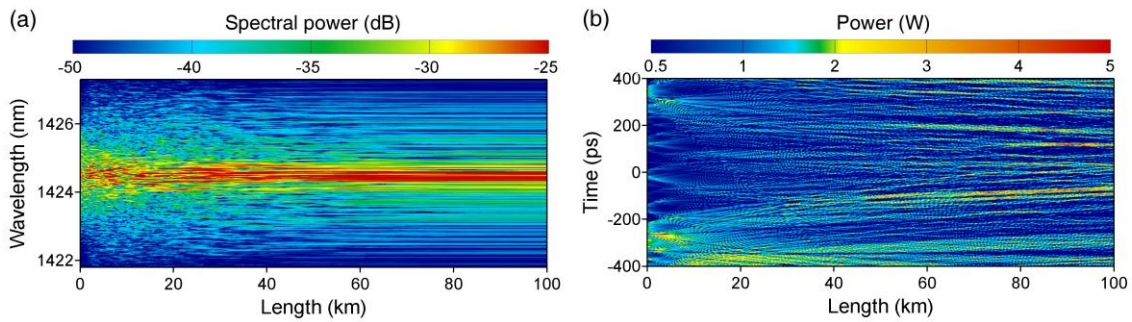


Figure 3. Evolution of the signal spectrum and temporal shape along the fibre. (a) Computed power spectrum density evolution along the LEAF fibre, demonstrating a transition to very stable propagation with a distinctive asymptotic spectrum. **(b)** The corresponding spatio-temporal dynamics is shown over an interval of 800 ps. Here the fluctuating CW power $P(t, z)$ is normalized by the distance-dependent factor $P_{norm}(z) = P(0)\exp(\alpha z)$, where $\alpha = 0.25$ dB/km is the fibre loss. The two figures illustrate that while the temporal field structure is irregular, the spectrum propagation demonstrates remarkable stability.

The results of experiments and numerical simulations presented in Figs. 2 and 3 demonstrate spectral narrowing of CW radiation with simultaneous temporal fluctuations. The initial spectrum is converted to the double-scale distribution (a bell-shaped peak in the centre but with exponentially decaying spectral tails introducing a second scaling parameter in the spectral distribution) at the LEAF output both in experiment and in simulation (Fig. 2). A stable spectrum evolution (after approximately 50 km) along the LEAF fibre is shown in Fig. 3(a). We would

like to stress that the observed stabilization of the spectrum is a nontrivial nonlinear process. Intensive numerical modeling shows that this happens both in a fibre span with loss and in the corresponding lossless system. Spatio-temporal dynamics of the signal feature highly irregular intensity fluctuations (Fig. 3(b)). Despite visible irregularities of the temporal field distribution shown in Fig. 3 (b), in the spectral domain, this statistical steady state is very stable and may evolve without major changes over long distances. Due to the fact that multiple modes are involved in building this statistical equilibrium through nonlinear FWM interactions, the process calls for a kinetic description [13, 27]. We believe that this is an interesting and practically important experimental observation of the kinetic equilibrium in optical fibre [8, 10, 12, 13, 27].

We have performed a number of experiments with various fibres at different wavelengths along with extensive numerical modeling and conclude that we were able to observe the effect of nonlinear spectral narrowing only in the case of normal fibre dispersion (see Supplementary Note 1).

Qualitative analysis. First, let us try to explain qualitatively the physical mechanism underlying the spectral narrowing of a high-power field containing many longitudinal modes in normal dispersion fibre. The key idea came from the observation that the Raman laser output (with its double-peaked spectrum) being launched into the LEAF fibre resembles a 2-pump optical parametric amplifier with two spectrally separated pumps. Of course, there are no separate "pumps" and "signal" in this case; instead, the input field self-acts in re-distributing energy from the peripheral wavelengths - "pumps" to the central region - "signal". This is obviously only a qualitative picture that helps in understanding the main elementary mechanism of such self-pumping of the central wavelength region at the expense of the tails. Consider those effective "pumps" to be at frequencies ω_1 and ω_2 at the fibre input. Such effective "pumps" would amplify "signal" and "idler" with frequencies ω_3 and ω_4 , respectively. Consider, $\omega_1 < \omega_2$ and $\omega_3 < \omega_4$. Evidently, here "signal" and "idler" represent just two spectral components of the

same wave-packet that through FWM get energy from the tails of the spectrum ("pumps"). Notice that ω_3 and ω_4 are symmetric with respect to the center frequency $\omega_c = (\omega_1 + \omega_2)/2 = (\omega_3 + \omega_4)/2$, which is halfway between the two pump frequencies. As a matter of fact, the self-parametric amplification effect does not require a two-pump structure of the input field; similar spectral narrowing can be observed for input waves having a bell-shaped spectrum. This was conclusively confirmed by additional experiments and modeling (see discussion below). The particular example considered here is very useful for understanding the underlying principle, i.e. the two spectral peaks in the Raman laser output could be associated with the "pumps", whereas the spectral narrowing of the laser output as it propagates in the normal dispersion fibre could be associated with the "signal" and "idler" (or just "signal" if $\omega_3 = \omega_4$) amplification in an effective fibre OPA.

In this qualitative analysis, consider first the un-depleted pump case when signal and idler are small compared to the pumps $P_3 \ll P_0 = P_1 + P_2$ (for simplicity, as the analysis in this section is only qualitative, formulae here are given for the case when the idler is absent at $z=0$). The unsaturated single pass gain for signal G_3 may be written as [15, 17]:

$$G_3 = \frac{P_3(L)}{P_3(0)} = 1 + \left[\frac{\gamma P_0}{g} \sinh(gL) \right]^2, \quad (1)$$

with the idler gain being $G_4 = G_3 - 1$. Here, g is a parametric gain coefficient given by $g^2 = r^2 - (k/2)^2$, $r = \gamma P_0$, γ is nonlinearity coefficient. The gain coefficient reaches its maximum value when $k = \Delta\beta + \Delta\beta_{NL} = 0$, where k is the total propagation constant, $\Delta\beta = \beta(\omega_3) + \beta(\omega_4) - \beta(\omega_1) - \beta(\omega_2)$ is the propagation constant mismatch and $\Delta\beta_{NL} = \gamma P_0$ is the nonlinear contribution to the wavevector mismatch. The corresponding single pass signal gain is equal to:

$$G_{3,max} = 1 + [\sinh(\gamma P_0 L)]^2, \quad (2)$$

and for the idler:

$$G_{4,max} = [\sinh(\gamma P_0 L)]^2.$$

It is convenient to introduce the following notations: $\Delta\omega_s = \omega_3 - \omega_c$, $\Delta\omega_p = \omega_1 - \omega_c = \omega_c - \omega_2$.

To understand the effect of dispersion, we can expand the propagation constant mismatch in a

standard power series in terms of $\Delta\omega_s$ and $\Delta\omega_p$ [15, 17]: $\Delta\beta = 2 \sum_{m=1}^{\infty} \frac{\beta_{2m}}{(2m)!} [(\Delta\omega_s)^{2m} - (\Delta\omega_p)^{2m}]$,

where β_{2m} are even derivatives of $\beta(\omega)$ at ω_c . Consider only the main term in this expansion

assuming that $\beta_4 \ll \beta_2$, i.e. $\Delta\beta \approx \beta_2 [(\Delta\omega_s)^2 - (\Delta\omega_p)^2]$. The shape of the gain spectrum and

location of the gain maximum in the spectral domain are given by the condition of phase

matching:

$$k = 0 \Rightarrow [(\Delta\omega_s)^2 - (\Delta\omega_p)^2] = -\gamma P_0 / \beta_2 \quad (3)$$

Equation (3) provides a reasonable qualitative explanation of why the sign of the dispersion

does matter in the considered experiment: when fibre dispersion is normal $\beta_2 > 0$, the gain

maximum is located between the pumps, $\Delta\omega_s < \Delta\omega_p$. On the other hand, when fibre dispersion is

anomalous $\beta_2 < 0$, the gain maximum is located outside the area between the pumps, in the

frequency domain $\Delta\omega_s > \Delta\omega_p$ as illustrated by Fig. 4(a). Figure 4(a) depicts the signal parametric

gain G_3 [dB] as a function of distance $\Delta\lambda$ between the pumps and signal wavelength. Black

lines show the wavelengths of the pumps. As one can see, in the normal dispersion regime, the

gain spectrum is bell-shaped with the maximum amplification in its central part. When

dispersion is anomalous, symmetric gain maxima are always located outside the area between

the pumps, which effectively leads to significant spectrum broadening.

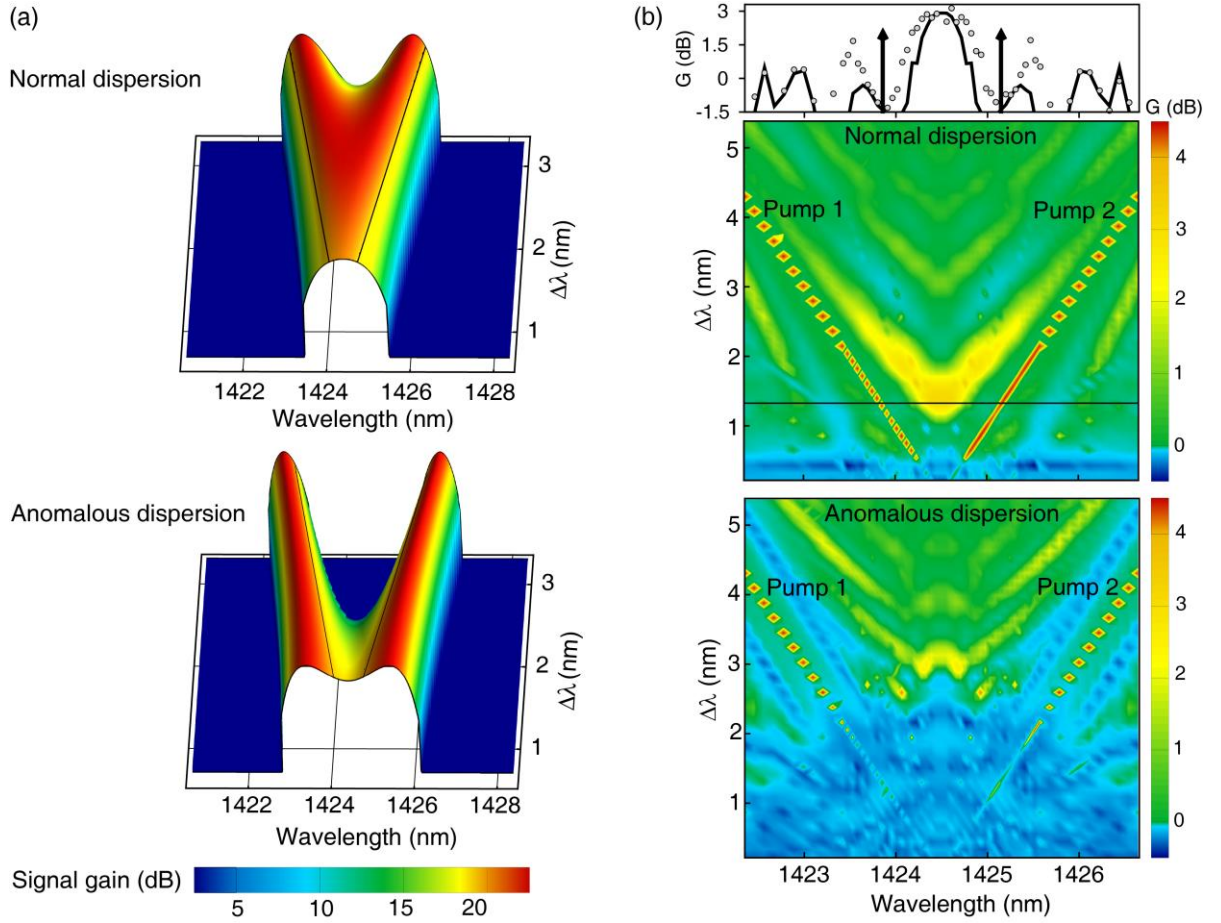


Figure 4. Signal gain spectra as a function of pumps wavelengths spacing. (a) 4-wave model, $P_0(0) = 1.5$ W, $L = 1$ km. The unsaturated single pass gain for signal G_3 is shown. Black lines show the corresponding wavelengths of the pumps. (b) NLSE model, $P_0(0) = 1.5$ W, $P_3(0) = 300$ mW, $P_4(0) = 0$, $L = 1$ km. The projection at the top is related to the normal dispersion case: black solid line – deterministic phases of waves; grey circles – averaging over 600 sets of random phases.

Note that, for a central frequency gain, when signal coincides with idler $\Delta\omega_s = 0$, we deal with degenerate OPA and signal amplification should be considered in the framework of the degenerate OPA model. The qualitative analysis presented in this section explains the difference between normal and anomalous dispersion propagation regimes. However, this simple model does not take into account pump depletion and the generation of additional waves through FWM. This changes the quantitative characteristics of the SPA process and requires a more accurate analysis that is presented in the following section.

Gain analysis in the nonlinear Schrödinger equation model. Certainly, the 4-wave model above gives only a qualitative picture; many other frequency components are generated and interact with each other due to four-wave mixing in the process under consideration. Some of these waves may be well phase-matched and so may reach levels comparable with the "signal". To give a more realistic evaluation of the self-parametric amplification, we now use the nonlinear Schrödinger equation (NLSE) to obtain the signal amplification spectrum in the presence of parasitic FWM components depleting the effective gain. Figure 4(b) shows the signal gain spectrum corresponding to the two-pump fibre OPA with varying distance between the pumps. Here the total pump power is 1.5 W, the signal CW power at the fibre input equals to 300 mW and the idler is absent at $z = 0$. The gain spectrum is still bell-shaped if the distance between the pumps is properly chosen (see Fig. 4(b), inset) and maximum amplification is achieved in the frequency band between the pumps.

Note that previously we considered an ideal case - a phase-insensitive parametric amplifier. The real laser output has the form of a multimode light field without phase locking; thus, self-parametric amplification of such a field is phase-sensitive. To study the impact of the effect of random initial phases, we have performed additional simulations. We considered signal and idler with equal powers (300 mW total power) at the fibre input and the relative phase difference between the four involved light waves at the fibre input $\theta(0) = \varphi_3(0) + \varphi_4(0) - \varphi_1(0) - \varphi_2(0)$ was assumed to be a random value with a uniform probability distribution bounded between $-\pi$ and π . Statistical analysis was done with 600 different sets of the random phases. A statistical signal gain spectrum averaged over the 600 sets is shown by dashed line grey circles in Fig. 4 right top. It has a characteristic high peak at the central frequency similar to the simplified 4-wave model.

Although we have shown that the maximum signal amplification can be achieved near the central frequency, new spectral components still could be amplified simultaneously with the signal and lead to the broadening of the laser spectrum. To investigate pump energy transfer along the fiber, we consider signal amplification at the central frequency (signal coincides with

idler $\omega_c = \omega_3 = \omega_4$). To estimate a value of the FWM product during the signal amplification, we introduce the dimensionless function $F(\Delta\lambda, \theta(0))$, defined as the ratio between pump energy transferred to signal at the frequency $\omega = \omega_3$ and pump energy transferred to other frequencies due to FWM: $F = \Delta P_s / P_{FWM}$, where $\Delta P_s = P_3(L) - P_3(0)$ and $P_{FWM} = P_0(0) + P_3(0) - P_0(L) - P_3(L)$. $F(\Delta\lambda, \theta(0))$ is a figure of merit indicating how effectively pump energy transfers to signal, i.e. efficiency of signal amplification. $F=0$ corresponds to $G_3=0$, i.e. no amplification for the ω_3 signal, whereas F tends to infinity when the only spectral component amplified is the ω_3 signal.

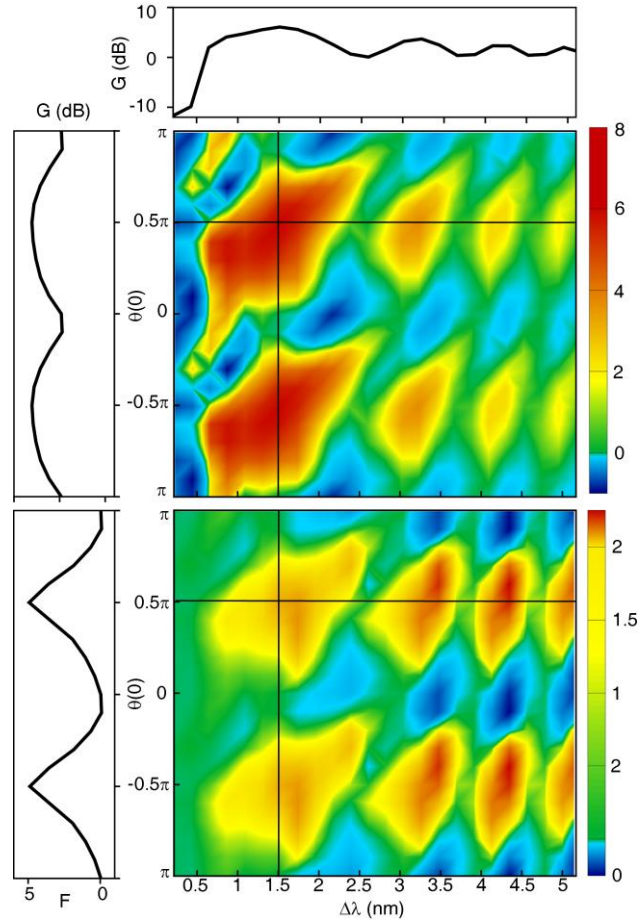


Figure 5. Estimate of the FWM product during the signal amplification. (Top) Dependence of the signal gain G [dB] on relative phase difference $\theta(0)$ and wavelength spacing between two pumps $\Delta\lambda$. **(Bottom)** Dependence of the function $F = \Delta P_s / P_{FWM}$ on relative phase difference $\theta(0)$ and wavelength spacing between two pumps $\Delta\lambda$.

Figure 5 shows value of the signal gain $G = 10 \log_{10} (P_s(L) / P_s(0))$ and dimensionless function F (bottom row) in the plane of parameters $\Delta\lambda - \theta(0)$. It can be seen, the FWM product can be

neglected if the spectral distance between the pumps is properly chosen (undesirable FWM product is minimized and all the pump energy transfers to the signal).

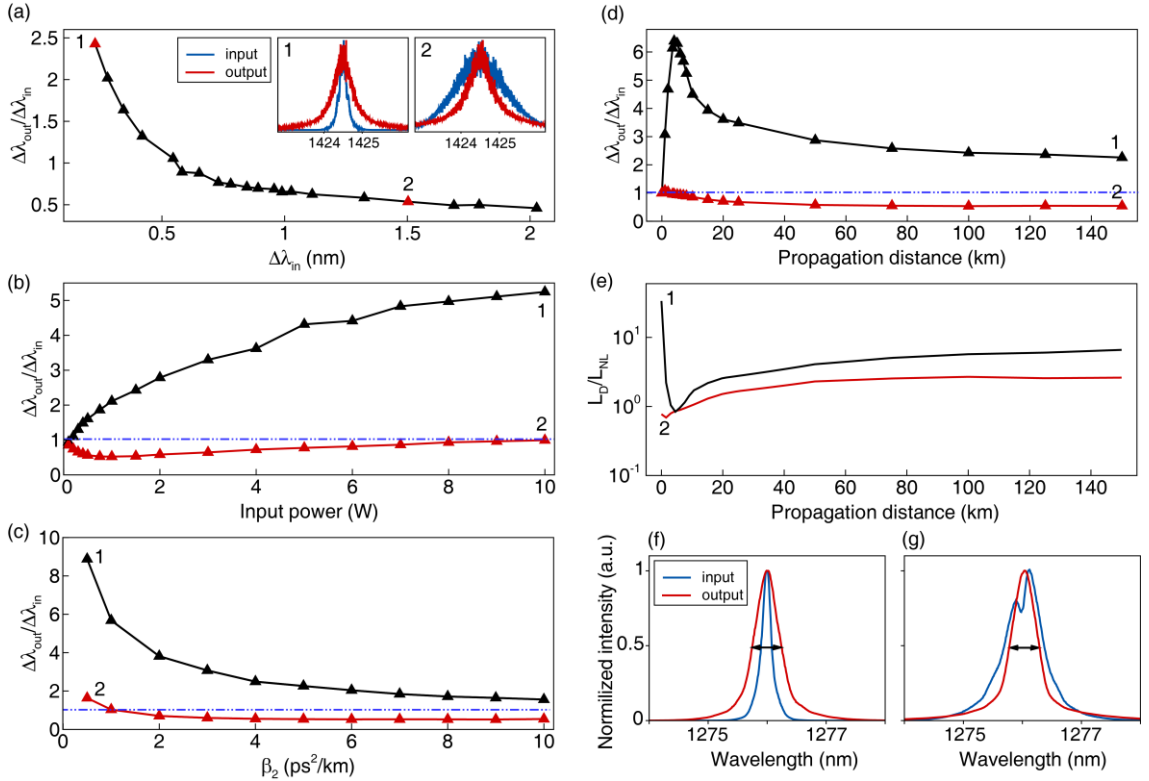


Figure 6. Theoretical evolution of the spectral broadening factor. Dependence of the broadening factor $\Delta\lambda_{out} / \Delta\lambda_{in}$ on (a) initial spectrum width $\Delta\lambda_{in}$ after 100 km of LEAF, $P_0 = 1.5$ W, lossless fibre. (Inset) Spectrum shapes before and after signal propagation in 100 km of LEAF, corresponding to the points marked “1” and “2”; (b) pump power, corresponding to the points marked “1” and “2”, $L = 100$ km; (c) group delay dispersion, corresponding to the points marked “1” and “2”, $L = 100$ km, $P_0 = 1.5$ W; (d) fibre length, corresponding to the points marked “1” and “2”, $P_0 = 1.5$ W. (e) Scaling of L_d / L_{NL} along the propagation distance, $P_0 = 1.5$ W. (f,g) Experimentally measured input and output spectra of 1276-nm light propagating in 100 km of SMF-28 vs. input power (f) $P_0 = 0.7$ W, (g) $P_0 = 1.3$ W.

Discussion

An interesting question is: what are the conditions for spectral compression and broadening in normal dispersion fibre? In Figure 6 we considered the broadening factor $\Delta\lambda_{out} / \Delta\lambda_{in}$ as a function of: initial spectral width, power, fibre dispersion and cavity length. Figure 6(a) depicts the evolution of the broadening factor $\Delta\lambda_{out} / \Delta\lambda_{in}$ with an initial spectrum width $\Delta\lambda_{in}$ in numerical simulations. When the spectrum width at $z = 0$ is less than 0.5 nm, we still observe spectrum broadening in a 100-km long fibre. However, if $\Delta\lambda_{in}$ exceeds 0.5 nm, spectrum

narrowing takes place. We verified that this effect is observed both in lossy and lossless cases (see details in Supplementary Note 2). We also studied the impact of dispersion (Supplementary Note3) and statistics of the compressing signal (Supplementary Note 4). In Figs. 6(b)-(e) we consider in more detail two different points along the line, corresponding to spectrum broadening and narrowing (marked as ``1" and ``2" in Fig. 6(a)). For $\Delta\lambda_m = 0.23$ nm, the broadening factor first monotonically increases with the fibre length L as long as it is shorter than 5 km (Fig. 6(d)). With further increase of propagation distance, the initial rise is followed by a decrease. This kind of evolution of a multimode CW field was previously observed in [31]. Scaling of L_d / L_{NL} along the propagation distance is shown in Figure 6(e). Spectral broadening occurs when the dispersion length at the fibre input is much greater than the nonlinear length. On the other hand, when dispersion length becomes comparable with the nonlinear length, we observe nonlinear spectral narrowing. The observed nonlinear spectral broadening depends on the ratio of the dispersive and nonlinear lengths L_d / L_{NL} . Therefore, light with a broader bandwidth can be also compressed provided that after rescaling of parameters the factor L_d / L_{NL} is the same as in the studied examples.

We additionally experimentally verified that the RFL spectrum is also narrowing when transmitted through other fibres with normal dispersion, as shown in Fig. 6(f,g). The laser radiation generated at 1276 nm was launched into the same 100-km length of SMF-28 which has normal dispersion at this wavelength ($\beta_2 = 3.1$ ps²/km, $\gamma = 1.8$ W⁻¹km⁻¹). We observed spectral narrowing both in experiment and simulation. In the experiment, a narrow and low power (0.7 W) RFL spectrum becomes broader after propagation in SMF (Fig. 6(f)); however, when initial width and power increases (1.3 W), one can see compression (Fig. 6(g)) and formation of a stable spectrum.

The remarkable spectral stability of the evolved state (in normal dispersion fibre) despite a random temporal behaviour indicates that we observe an asymptotic kinetic regime that resulted from the optical wave turbulence of a multitude of elementary waves in the nonlinear system

considered [8, 10, 12, 13, 35]. It is also worth pointing out that this surprising finding that the evolved spectral distribution does not change appreciably with propagation may potentially be exploited in fibre lasers and optical telecommunications. In fibre lasers, nonlinear compression may lead to increased spectral brightness compared to systems using direct spectral filtering, avoiding additional losses inevitable with filters. In optical communications, spectrally stable nonlinear propagation regimes may lead to new techniques of mitigation of nonlinear transmission impairments that are a major challenge in modern high-capacity systems.

Conclusion

We have presented a new self-action effect that may occur during high-power wave propagation in normal dispersion fibre - self-parametric amplification or inverse four-wave mixing that manifests itself as a spectral compression of light. This is different from compression of pre-chirped coherent pulses [36-41]. Observed effect is the result of a nonlinear energy redistribution from the tails of signal spectrum to the central region. This can be considered as an effective self-parametric amplification of the central part of the wave packet spectrum by the peripheral "pumps". The simple theory of self-parametric amplification presented explains all the key features observed in the experiments and full numerical modelling. We believe that the remarkable stability of the observed spectral field distribution may offer new interesting applications in high power fibre lasers and optical telecommunications.

Methods

Propagation in LEAF: Signal propagation down the LEAF fibre has been modelled using the NLS equation with losses [2]:

$$\frac{\partial A}{\partial z} = -i \frac{\beta_2}{2} \frac{\partial^2 A}{\partial t^2} + i\gamma |A|^2 A - \frac{\alpha}{2} A, \quad (\text{M1})$$

where $A(z, t)$ is the electric field envelope, β_2 is the second-order dispersion coefficient at the central frequency ω_0 , $\gamma = n_2 \omega_0 / (c A_{eff})$ is the Kerr nonlinearity coefficient with the nonlinear refractive index n_2 and effective fibre cross-section area A_{eff} for the fundamental mode and α is the fibre attenuation coefficient. The equation has been solved using the split-step Fourier transform method. The following fibre parameters are used in the simulations: $\beta_2 = 4.3 \text{ ps}^2/\text{km}$, $\gamma = 2.16 \text{ W}^{-1}\text{km}^{-1}$, $\alpha = 0.25 \text{ dB/km}$.

Raman fibre laser: To model the laser generation, we use a NLSE-based model previously reported to be efficient for modeling of RFLs [32]:

$$\begin{aligned} \frac{\partial A_p^\pm}{\partial z} &= -\frac{i}{2} \beta_{2p} \frac{\partial^2 A_p^\pm}{\partial t^2} + i \gamma_p \left[|A_p^\pm|^2 + (2 - f_R) |A_s^\pm|^2 \right] A_p^\pm - \frac{g_p}{2} \left(|A_s^+|^2 + |A_s^-|^2 \right) A_p^\pm - \frac{\alpha_p}{2} A_p^\pm \\ \frac{\partial A_s^\pm}{\partial z} &= \left(\frac{1}{v_s} - \frac{1}{v_p} \right) \frac{\partial A_s^\pm}{\partial t} - \frac{i}{2} \beta_{2s} \frac{\partial^2 A_s^\pm}{\partial t^2} + i \gamma_s \left[|A_s^\pm|^2 + (2 - f_R) |A_p^\pm|^2 \right] A_s^\pm + \frac{g_s}{2} \left(|A_p^+|^2 + |A_p^-|^2 \right) A_s^\pm - \frac{\alpha_s}{2} A_s^\pm \end{aligned} \quad (\text{M2})$$

The boundary conditions describe the pump input and the reflection of the optical field from the fibre Bragg gratings:

$$\begin{aligned} A_p^+(0, t) &= A_{in}, \quad A_p^-(L, \omega) = \sqrt{R_p(\omega)} A_p^+(L, \omega) \\ A_s^+(0, \omega) &= \sqrt{R_{in}(\omega)} A_s^-(0, \omega), \quad A_s^-(L, \omega) = \sqrt{R_{out}(\omega)} A_s^+(L, \omega) \end{aligned}$$

where $R_{in}(\omega)$ and $R_{out,p}(\omega)$ are the reflectivities (with respect to power) at the left and right cavity ends, respectively.

The model describes spectral broadening during one round trip and the building of a steady state over many round trips. We integrated equations (M2) along z using the split-step Fourier transform method and an iterative procedure similar to that used for modeling of Brillouin fibre lasers [34]. For example, to integrate the equation for $A_{s,p}^\pm(z, t)$, we substituted into the equation $A_{s,p}^\pm(z, t)$ obtained on a previous iteration and so on. The generation becomes stable after 10^2 – 10^4 round trips, depending on the power.

References

1. Stolen, R.H. The early years of fiber nonlinear optics. *J. Lightwave Technol.* **26**, 1021-1031 (2008).
2. Agrawal, G.P. *Nonlinear Fiber Optics* (Oxford, UK, 2007).
3. Boyd, R.W. *Nonlinear Optics* (Academic Press, 2003).
4. Toulouse, J. Optical nonlinearities in fibers: Review, recent examples, systems applications. *J. Lightwave Technol.* **23**, 3625-3641 (2005).
5. Dudley, J.M. & Taylor, J.R. Ten years of nonlinear optics in photonic crystal fibre. *Nature Photon.* **3**, 85-90 (2009).
6. Garmire, E. Nonlinear optics in daily life. *Opt. Express* **21**, 30532-30544 (2013).
7. Solli, D. R., Ropers, C., Koonath, P. & Jalali, B. Optical rogue waves. *Nature* **450**, 1054-1057 (2007).
8. Turitsyna, E. G. *et al.* The laminar-turbulent transition in a fibre laser. *Nature Photon.* **7**, 783-786 (2013).
9. Kibler, B. *et al.* The Peregrine soliton in nonlinear fibre optics. *Nature Phys.* **6**, 790-795 (2010).
10. Turitsyn, S.K. *et al.* Random distributed feedback fibre laser. *Nature Photon.* **4**, 231-235 (2010).
11. Turitsyn, S.K., Bale, B. & Fedoruk, M.P. Dispersion-managed solitons in fibre systems and lasers. *Phys. Rep.* **521**, 135-203 (2012).
12. Turitsyn, S.K. *et al.* Random distributed feedback fibre lasers. *Phys. Rep.* **542**, 133-193 (2014).
13. Picozzi, A. *et al.* Optical wave turbulence: Toward a unified nonequilibrium thermodynamic formulation of statistical nonlinear optics. *Phys. Rep.* **542**, 1-132 (2014).
14. Stolen, R.H., Phase-matched-stimulated four-photon mixing in silica-fiber waveguides. *IEEE J. Quantum Electron.* **11**, 100-103 (1975).

15. Marhic, M. E. *Fiber Optical Parametric Amplifiers, Oscillators and Related Devices*. (Cambridge University Press, 2007).
16. Hansryd, J., Andrekson, P.A., Westlund, M., Li, J. & Hedekvist, P.O., Fiber-based optical parametric amplifiers and their applications. *J. Sel. Top. Quantum Electron.* **8**, 506-520 (2002).
17. Radic, S. & McKinstrie, C.J. Two-pump fiber parametric amplifiers. *Opt. Fiber Technol.* **9**, 7-23 (2003).
18. McKinstrie, C. & Radic, S. Phase-sensitive amplification in a fiber. *Opt. Express* **12**, 4973-4979 (2004).
19. McKinstrie, C.J., Radic, S. & Gnauck, A.H. All-optical signal processing by fiber-based parametric devices. *Opt. Photonics News* 18, 34-40 (2007).
20. Marhic, M.E. *et al.* Fiber optical parametric amplifiers in optical communication systems, *Laser & Photon. Rev.* **9**, 50–74 (2015).
21. Tong, Z. *et al.* Towards ultrasensitive optical links enabled by low-noise phase-sensitive amplifiers. *Nature Photon.* **5**, 430-436 (2011).
22. Slavik, R. *et al.* All-optical phase and amplitude regenerator for next-generation telecommunications systems. *Nature Photon.* **4**, 690-695 (2010).
23. Karpov, V.I., Clements, W.R.L., Dianov, E.M. & Papernyi, S. B. High-power 1.48 micrometer phosphoro-silicate-fiber-based laser pumped by laser diodes. *Canadian Journal of Physics* **78**, 407-413 (2000).
24. Bouteiller, J.-C. Spectral modeling of Raman fiber lasers. *PTL* **15**, 1698-1700 (2003).
25. Suret, P. & Randoux, S. Influence of spectral broadening on steady characteristics of Raman fiber lasers: from experiments to questions about the validity of usual models. *Opt. Commun.* **237**, 201-212 (2004).
26. Turitsyn, S.K. *et al.* Modeling of CW Yb-doped fiber lasers with highly nonlinear cavity dynamics. *Opt. Express* **19**, 8394-8405 (2011).

27. Babin, S., Churkin, D., Ismagulov, A., Kablukov, S. & Podivilov, E., Four-wave-mixing-induced turbulent spectral broadening in a long Raman fiber laser. *J. Opt. Soc. Am. B* **24**, 1729-1738 (2007).
28. Turitsyn, S.K. *et al.* Optical wave turbulence, in *World Scientific Series on Nonlinear Science Series A: Volume 83, Advances in Wave Turbulence*, V. Shrira and S. Nazarenko, eds. (World Scientific, 2013).
29. Babin, S. *et al.* Turbulent broadening of optical spectra in ultralong Raman fiber lasers. *Phys. Rev. A* **77**, 033803 (2008).
30. Turitsyna, E.G., Falkovich, G., Mezentsev, V.K. & Turitsyn, S.K. Optical turbulence and spectral condensate in long-fiber lasers. *Phys. Rev. A* **80**, 031804 (2009).
31. Barviau, B., Randoux, S., & Suret, P. Spectral broadening of a multimode continuous-wave optical field propagating in the normal dispersion regime of a fiber. *Opt. Lett.* **31**, 1696-1698 (2006).
32. Churkin, D., Smirnov, S. & Podivilov, E. Statistical properties of partially coherent cw fiber lasers. *Opt. Lett.* **35**, 3288-3290 (2010).
33. Paramonov, V.M., Kurkov, A. S., Medvedkov, O. I., Gruk, D. A. & Dianov, E. M. Two-frequency fibre Raman laser. *Quantum Electron.* **34**, 213-215 (2004).
34. Preda, C.E., Fotiadi, A. A. & Mégret, P. Numerical approximation for Brillouin fiber ring resonator. *Optics Express* **20**, 5783-5788 (2012).
35. Churkin, D.V. *et al.* Wave kinetics of random fibre lasers, *Nature Communications* **6**:6214 (2015).
36. Sidorov-Biryukov, D.A. *et al.* Spectral narrowing of chirp-free light pulses in anomalously dispersive, highly nonlinear photonic-crystal fibers. *Opt. Express* **16**, 2502-2507 (2008).
37. Cundiff, S. T. *et al.* Propagation of Highly Chirped Pulses in Fiber-Optic Communications Systems. *J. Lightwave Technol.* **17**, 811-816 (1999).

38. Washburn, B.R., Buck J.A. & Ralph, S.E. Transform-limited spectral compression due to self-phase modulation in fibers. *Opt. Lett.* **25**, 445-447 (2000).
39. Planas, S.A., Pires Mansur, N.L., Brito Cruz, C.H. & Fragnito, H.L. Spectral narrowing in the propagation of chirped pulses in single-mode fibers. *Opt. Lett.* **18**, 699-701 (1993).
40. Oberthaler, M. & Höpfel, R.A. Spectral narrowing of ultrashort laser pulses by self-phase modulation in optical fibers. *Appl. Phys. Lett.* **63**(8), 1017–1019 (1993).
41. Nishizawa, N., Takahashi, K., Ozeki, Y. & Itoh, K. Wideband spectral compression of wavelength-tunable ultrashort soliton pulse using comb-profile fiber. *Opt. Express* **18**, 11700-11706 (2010)

Acknowledgements

The authors acknowledge financial support from ERC project ULTRALASER (267763); Ministry of Education and Science of the Russian Federation (14.B25.31.0003 and 14.578.21.0029); the Russian Science Foundation (14-21-00110) (work of A.E.B). The authors also thank Dr. E. V. Podivilov for fruitful discussions.

Author contributions

S.B.P initiated the study and did the experiments. A.E.B. designed and conducted the numerical modeling, S.K.T., A.E.B. and M.P.F. guided the theoretical and numerical studies. S.K.T., S.B.P., A.E.B., W.R.L.C and M.P.F. analyzed the data. S.K.T., A.E.B., S.B.P., and W.R.L.C wrote the paper.

Competing financial interests

The authors declare no competing financial interests.